TJNN Thai Journal of Nanoscience and Nanotechnology

# Tuning Electrical and Optical Properties of $SnO_2$ Films: Influence of Sb Dopant Concentration and Coating Layer in Spin-Coating Process

Thanaphon Kansaard[1,*], Jitpisoot Sawangjaeng[1], Kanokthip Boonyarattanakalin[1], Chakkaphan Wattanawikkam[2] and Russameeruk Noonuruk[2]

[1]*School of Integrated Innovative Technology, King Mongkut's Institute of Technology Ladkrabang, Bangkok, 10520, Thailand*
[2]*Division of Physics, Faculty of Science and Technology, Rajamangala University of Technology Thanyaburi, Pathum Thani, 12110, Thailand*

*Received: 27 May 2025, Revised: 24 June 2025, Accepted: 25 June 2025*

## Abstract

This study investigates the optical and electrical properties of antimony (Sb)-doped tin oxide ($SnO_2$), commonly referred to as ATO, transparent conducting thin films synthesized via a wet chemical route. The films were fabricated using a sol-gel method combined with spin-coating. The effects of Sb doping concentrations (1, 3, and 5 mol%) and the number of coating layers (5 and 10) on the films' properties were systematically examined. ATO films were deposited onto glass substrates at a constant spin speed of 2000 rpm, followed by calcination at 600 °C for 2 hours. X-ray diffraction (XRD) analysis confirmed the formation of a tetragonal $SnO_2$ structure with no secondary phases. Optical measurements revealed high transparency in the visible range, with transmittance values between 60% and 80%. The lowest resistivity of 0.16 Ω·m was achieved with 5 mol% Sb and 10 coating layers, which also corresponded to the highest carrier concentration of $2 \times 10^9$ $cm^{-3}$, as determined by Hall effect measurements. These results demonstrate that optimized ATO films possess desirable properties for electronic and optoelectronic device applications.

**Keywords:** Sb-doped $SnO_2$ film, Sol-gel, Spin coating technique

## 1. Introduction

Today, various technologies play a crucial role in enhancing the convenience and functionality of daily life, particularly in the field of electronic and optoelectronic devices such as smartphones, tablets, computers, displays, and solar cells. These devices are essential for communication, productivity, and daily activities, and incorporate key components like liquid crystal displays (LCDs), organic light-emitting diodes (OLEDs), processors, memory units, motherboards, and optical sensors. Many of these applications demand materials with both high optical transparency and excellent electrical conductivity. Metals are commonly used as conductive materials due to their abundance of free charge carriers resulting from their unique electronic band structures. However, their intrinsic opacity limits their use in applications requiring transparency. In contrast, many metal oxide materials exhibit good optical transparency due to their wide band gaps, which typically give them insulating properties [1]. To meet the demand for materials that are both conductive and transparent, transparent conductive oxides (TCOs) have been developed and are widely used in optoelectronic applications, including solar cells and display technologies, due to their combined electrical and optical performance [2]. In recent years, research and development efforts have focused on utilizing TCO thin films as transparent electrodes in solar cells. These films allow sunlight to reach the active layer while simultaneously conducting electrons to the external circuit. Among the most studied TCO materials are indium tin oxide (ITO), aluminum-doped zinc oxide (AZO), and antimony-doped tin oxide (ATO). These candidates exhibit favorable optical and electrical properties [3]. However, ITO usage is limited by the scarcity of indium, resulting in high production costs and making it less suitable for large-scale manufacturing [4]. Although AZO offers a more cost-effective alternative, it presents challenges such as higher electrical resistance and more complex fabrication requirements [5]. ATO has emerged as a promising alternative

*Corresponding Author: tkansaard@gmail.com*

TCO due to its good electrical conductivity, high optical transparency, chemical stability, mechanical durability, and thermal resistance [6]. ATO thin films can be fabricated using various methods, including chemical vapor deposition (CVD), sputtering, spray pyrolysis, and sol-gel spin-coating. Among these techniques, the sol-gel method is particularly attractive due to its simplicity, low cost, and suitability for large-area and flexible substrate applications without the need for a vacuum system [7]. Doping $SnO_2$ with antimony (Sb) enhances its electrical properties by increasing the free carrier concentration and enables absorption in the near-infrared (NIR) region through localized surface plasmon resonance (LSPR) [8]. This characteristic is especially useful for thermal shielding in electronic and energy-efficient devices.

This research focuses on investigating the effects of varying Sb dopant concentrations (1–5 mol%) and the number of coating layers on the properties of ATO thin films prepared by a simple wet chemical sol-gel and spin-coating method, followed thermal treatment process. The objective is to identify optimal conditions that result in superior electrical conductivity and optical transparency, with enhanced capability to block near-infrared radiation. The structural, morphological, optical, and electrical properties of the ATO thin films were analyzed to evaluate their potential for future optoelectronic applications.

## 2. Experimental

Pristine and Sb-doped $SnO_2$ thin films with varying Sb concentrations (0, 1, 3, and 5 mol%) were prepared using a sol-gel wet chemical method combined with spin-coating. Tin(IV) chloride pentahydrate ($SnCl_4 \cdot 5H_2O$, Sigma-Aldrich) was used as the precursor for the host material and dissolved in absolute ethanol at a concentration of 10 mM. For Sb doping, antimony trichloride ($SbCl_3$) was dissolved in deionized (DI) water at the desired concentrations (1–5 mol%). The two precursor solutions were mixed and stirred continuously at room temperature until a clear solution was obtained. To initiate gelation, 1 mL of diethanolamine (DEA) was added dropwise as a gel-forming agent. The mixture was then heated and stirred at 75 °C for 2 hours to reduce the solvent volume from 50 mL to approximately 35 mL, followed by aging at room temperature to complete gelation. The resulting sol-gel solution was deposited onto pre-cleaned glass substrates using a spin-coating technique at a constant speed of 2000 rpm for 30 seconds. Each coated layer was baked at 110 °C for 25 minutes to evaporate residual solvents. This process was repeated until the desired number of layers (5 or 10) was achieved. All as-deposited films were then subjected to calcination in a conventional furnace at 600 °C for 2 hours to complete the crystallization process.

The crystalline structure of the films was characterized by X-ray diffraction (XRD) using a Rigaku SmartLab diffractometer with Cu Kα radiation (λ = 1.54 Å). Surface morphology and film thickness were analyzed using a field emission scanning electron microscope (FESEM, JEOL JSM-7001F). Cross-sectional imaging was used to determine the thickness, while elemental composition was examined using energy-dispersive X-ray spectroscopy (EDX). Optical properties were evaluated using a UV–VIS–NIR diffuse reflectance spectrophotometer (HITACHI UH1450). Electrical properties were measured using Hall effect characterization (ECOPIA HMS-3000, NSTDA) configured in the van der Pauw geometry. Measurements were conducted in air at room temperature on 1 × 1 $cm^2$ samples, with a current of 0.1 mA, a magnetic field strength of 0.55 T, a measurement interval of 0.1 s, and a total of 1000 readings per sample.

## 3. Result and discussion

### 3.1 Crystallinity

The crystalline structure of the Sb-doped $SnO_2$ thin films was analyzed using X-ray diffraction (XRD), as shown in Fig. 1. All samples exhibited diffraction peaks characteristic of the tetragonal rutile structure of $SnO_2$, with prominent reflections at $2\theta = 26.6°$, 33.8°, 37.9°, and 51.7° corresponding to the (110), (101), (200), and (211) crystallographic planes, respectively [CSD: 16635]. These results confirm that the incorporation of Sb dopant ions did not result in the formation of secondary phases, even at higher doping concentrations. However, as the Sb concentration increased, a noticeable decrease in the

intensity of the diffraction peaks was observed. This reduction in peak intensity suggests that Sb doping hinders the crystallinity of the $SnO_2$ films. The decrease in crystallinity is likely due to the introduction of point defects, such as interstitial or substitutional Sb ions replacing Sn sites in the lattice. Given that the ionic radius of $Sb^{5+}$ (0.60 Å) is smaller than that of $Sn^{4+}$ (0.69 Å), such substitution induces lattice distortion and structural disorder [9]. This distortion is also evidenced by the slight shifts in lattice parameters, as presented in Table 1.

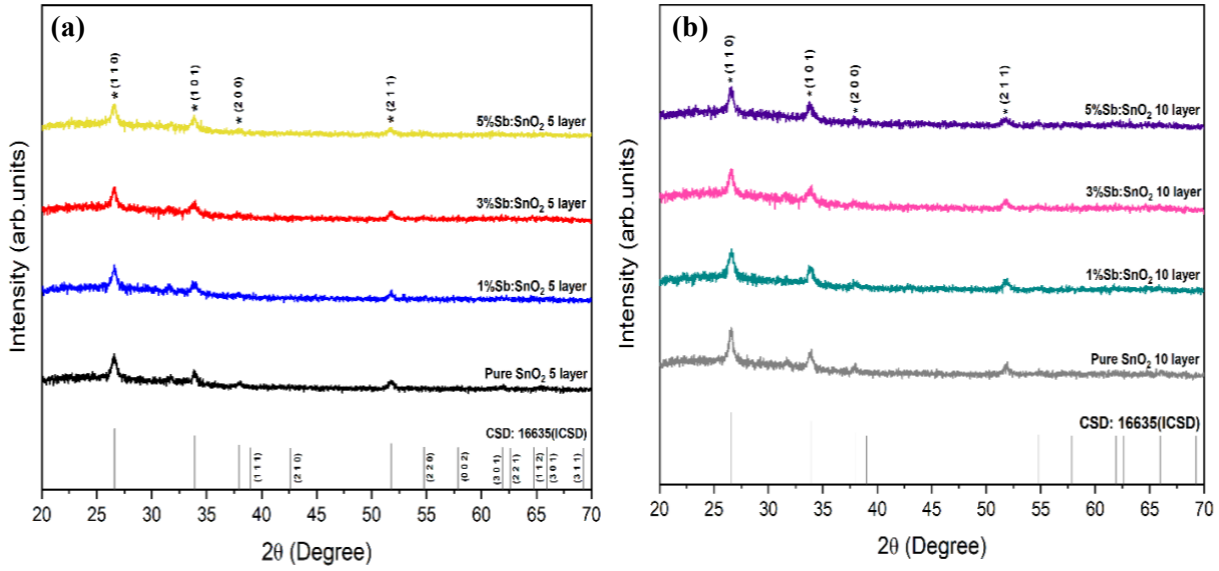


**Fig. 1.** X-rays diffraction spectra of all films (a) 5 layers and (b) 10 layers of coating

Additionally, the average crystallite size was found to decrease with increasing Sb content. This trend further supports the notion that Sb dopant ions inhibit crystal growth, likely by disrupting the regular lattice arrangement or introducing internal strain within the crystal structure [10]. The relationship between Sb concentration and crystallite size is summarized in Table 1. Moreover, crystalline structure observation was conducted on the slightly changed crystalline size after the Sb dopant on tin oxide thin films, as calculated by Scherrer's equation (1). Additionally, the calculation of the lattice parameters of the tetragonal structure and lattice strain were evaluated by equations (2) and (3), which results are illustrated in Table 1

$$D = \frac{0.9\lambda}{\beta \cos\theta} \tag{1}$$

$$\frac{1}{d^2} = \left(\frac{h^2+k^2}{a^2}\right) + \left(\frac{l^2}{c^2}\right) \tag{2}$$

$$\varepsilon = \frac{\beta \cos\theta}{4} \tag{3}$$

When $D$ is the crystal structure size (nm), λ is the wavelength of X-rays source (0.154 nm), β is the full width at half the maximum (FWHM) of the diffraction peak (rad), θ is the angle of incidence and reflection measured from the plane, $d$ is the distance between crystal planes (nm), $[h, k, l]$ is the miller indices of crystal lattice, a, c is the lattice parameters (Å) and ε is the internal stress within the crystal structure.

**Table 1.** Comparison of the crystalline size, lattice parameters, and lattice strain of the Sb-doped $SnO_2$ thin films with different Sb loading and spin coating layers.

| Specimens | Layers | Crystalline size (nm) (110) plane | Lattice parameter (Å) | | Lattice stain ($10^{-3}$) |
|---|---|---|---|---|---|
| | | | a = b | c | |
| pure $SnO_2$ | 5 | 12.14 | 4.74 | 3.16 | 2.2 |
| 1%Sb:$SnO_2$ | | 9.75 | 4.73 | 3.16 | 2.7 |
| 3%Sb:$SnO_2$ | | 6.73 | 4.74 | 3.19 | 3.9 |
| 5%Sb:$SnO_2$ | | 9.81 | 4.74 | 3.18 | 2.7 |
| pure $SnO_2$ | 10 | 15.92 | 4.74 | 3.19 | 1.6 |
| 1%Sb:$SnO_2$ | | 12.37 | 4.73 | 3.18 | 2.1 |
| 3%Sb:$SnO_2$ | | 10.59 | 4.73 | 3.17 | 2.4 |
| 5%Sb:$SnO_2$ | | 12.35 | 4.74 | 3.19 | 2.1 |

### 3.2 Optical analysis

The optical properties of the as-prepared Sb-doped $SnO_2$ thin films were investigated using a UV–Visible–Near Infrared (UV–VIS–NIR) diffuse reflectance spectrophotometer, as shown in Fig. 2. The pristine $SnO_2$ film exhibited the highest transmittance across the visible to near-infrared (NIR) spectral range, approximately 500–2600 nm. In contrast, the Sb-doped films displayed a decreasing trend in transmittance, particularly in the NIR region (750–2600 nm), with increasing Sb concentration. This reduction in NIR transmittance is attributed to the localized surface plasmon resonance (LSPR) effect, which arises from the increased free carrier concentration introduced by $Sb^{5+}$ doping. These free carriers are generated when $Sb^{5+}$ ions substitute for $Sn^{4+}$ ions or occupy interstitial sites within the $SnO_2$ lattice, leading to enhanced carrier density and plasmonic absorption in the NIR region [11]. The 5 mol% Sb-doped $SnO_2$ film exhibited the lowest NIR transmittance, which correlates with the highest free carrier concentration and is consistent with the observed improvement in electrical conductivity [12]. Additionally, films with a greater number of coating layers showed a significant decrease in overall transmittance. This reduction is primarily due to the increased film thickness, which enhances light absorption and scattering within the Sb:$SnO_2$ layers.

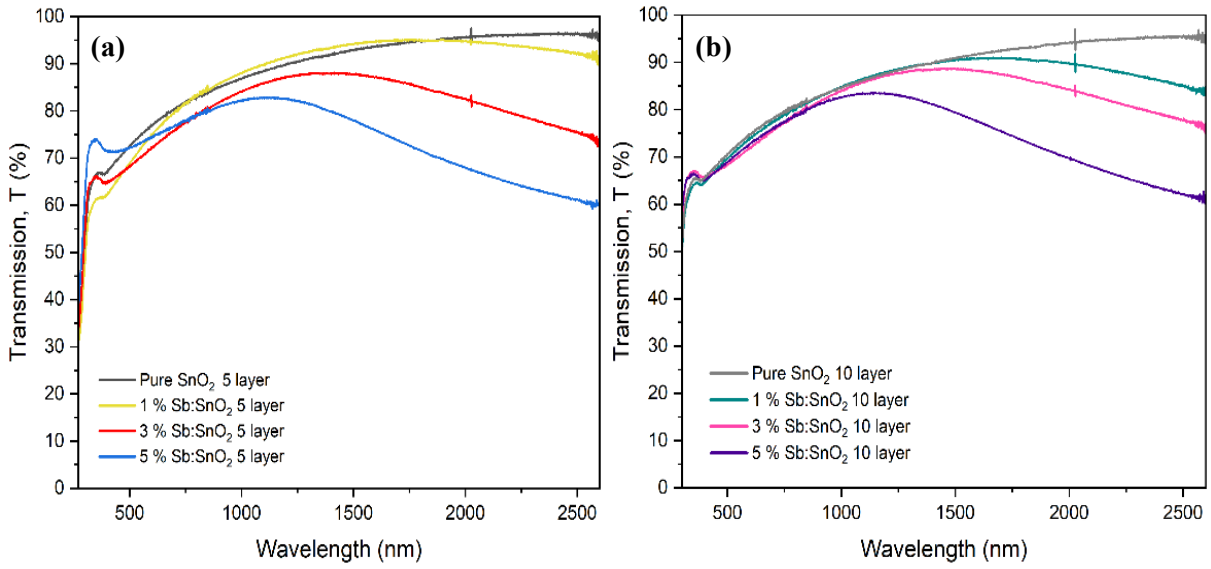


**Fig. 2.** Transmittance spectra of Sb-doped $SnO_2$ films varied Sb dopant concentration (0-5 mol%) and spin-coating layers (a) 5 layers and (b) 10 layers

The optical band gap ($E_g$) of the films was further evaluated using Tauc's plot method, as shown in Fig. 3. The pristine $SnO_2$ films exhibited band gap values of 3.90 eV and 3.88 eV for the 5-layer and 10-layer samples, respectively. Upon Sb doping, the optical band gap values showed a slight increase with increasing Sb concentration for both 5-layer and 10-layer films, as summarized in Table 2. This blue shift in band gap is likely due to the Burstein–Moss effect, where the increased carrier concentration leads to the filling of the lower energy states in the conduction band, resulting in an apparent widening of the band gap [3], [13].

$$(\alpha h\upsilon)^{\frac{1}{n}} = \beta(h\upsilon - E_g) \quad (4)$$

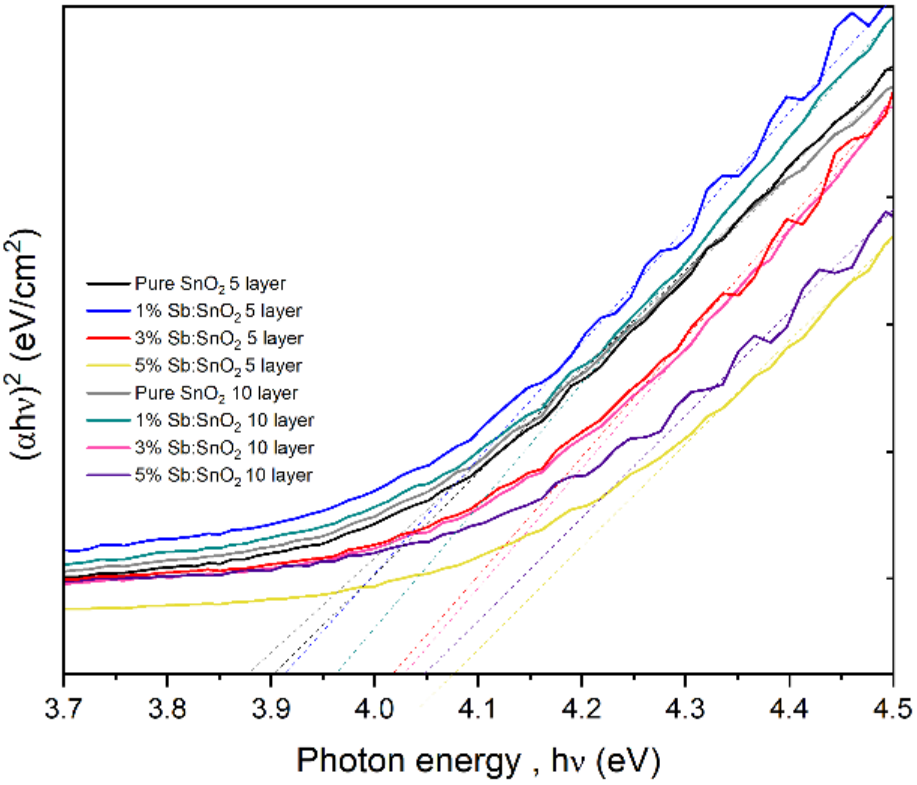


**Fig. 3.** Tauc plot calculation of all film samples with varied Sb dopant concentration and number of film coating layers

**Table 2.** Optical band gap value of Sb-doped $SnO_2$ samples evaluated by Tauc's plot calculation

| Samples | Layers | $E_g$ (eV) |
|---|---|---|
| pure $SnO_2$ | 5 | 3.90 |
| 1Sb: $SnO_2$ | | 3.92 |
| 3Sb: $SnO_2$ | | 4.02 |
| 5Sb: $SnO_2$ | | 4.08 |
| pure $SnO_2$ | 10 | 3.88 |
| 1Sb: $SnO_2$ | | 3.96 |
| 3Sb: $SnO_2$ | | 4.03 |
| 5Sb: $SnO_2$ | | 4.05 |

The increase in optical band gap ($E_g$) with higher Sb dopant concentrations is attributed to the rising free carrier density, which leads to a shift in the Fermi level ($E_f$), a phenomenon known as the Burstein-Moss shift (ΔEM). As the Sb doping level increases, more free electrons are introduced into the conduction band, causing the Fermi level to move upward. This upward shift effectively blocks the lower-energy electronic transitions, resulting in an apparent widening of the band gap [9], [11], [13]. Therefore, the higher $E_g$ values observed in the 10-layer of Sb-doped $SnO_2$ films can be correlated with an increased free carrier concentration, which is enhanced by both the greater number of coating layers and the higher Sb loading.

### 3.3 Electrical property

Based on the previous optical band gap ($E_g$) results, the 10-layer coated films exhibited higher band gap values, suggesting a higher free carrier concentration. Therefore, the electrical properties of the pristine and Sb-doped $SnO_2$ thin films (with 10 coating layers) were evaluated using the Hall effect measurement technique. The measured parameters included resistivity (ρ), conductivity (σ), carrier concentration (n), and carrier mobility (μ), as summarized in Fig. 4 and Table 3. The pristine $SnO_2$ film showed the highest resistivity of approximately $3.22 \times 10^3$ Ω·cm, corresponding to the lowest conductivity of $3.1 \times 10^{-4}$ $(\Omega \cdot cm)^{-1}$. In contrast, the Sb-doped $SnO_2$ films demonstrated a significant decrease in resistivity with increasing Sb content, yielding values of $1.04 \times 10^3$, $2.21 \times 10^{-1}$, and $1.61 \times 10^{-1}$ Ω·cm for 1%, 3%, and 5% Sb concentrations, respectively. Correspondingly, the conductivity increased with Sb loading, as shown in Fig. 4. The enhancement in electrical conductivity can be attributed to the substitutional incorporation of $Sb^{5+}$ ions into the $SnO_2$ lattice. Due to the smaller ionic radius of $Sb^{5+}$ (0.60 Å) compared to $Sn^{4+}$ (0.69 Å), this substitution introduces additional free carriers (electrons), which significantly improve conductivity. This highlights the critical role of Sb dopant concentration in tuning the electrical performance of $SnO_2$ films. Additionally, the trends in carrier concentration and Hall mobility are presented in Table 3. The undoped $SnO_2$ film exhibited the lowest carrier concentration of $1.42 \times 10^{12}$ $cm^{-3}$, while the 5% Sb-doped film reached a significantly higher value of $2.02 \times 10^{19}$ $cm^{-3}$. This dramatic increase confirms that $Sb^{5+}$ doping introduces free carriers, enhancing the electrical conductivity of the films [14]. In summary, increasing Sb dopant concentration effectively enhances the electrical properties of $SnO_2$ thin films by introducing more free carriers, thereby reducing resistivity and increasing both conductivity and carrier concentration.

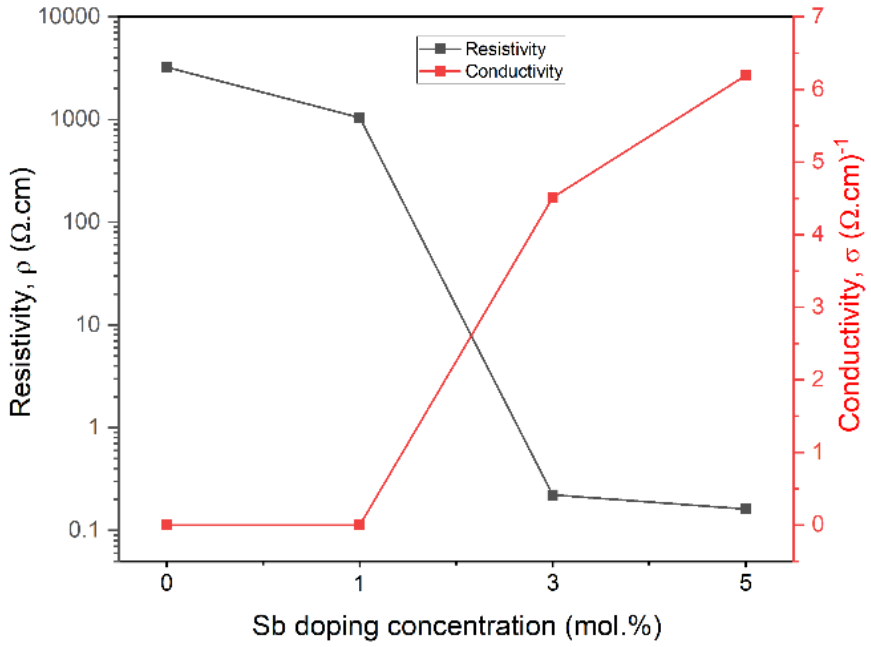


**Fig. 4.** Electrical conductivity and electrical resistivity of Sb-doped $SnO_2$ measured by Hall's effect technique in terms of electrical resistivity and conductivity

**Table 3.** Comparison of electrical parameters: electrical resistivity, electrical conductivity, carrier mobility, carrier concentration, and Hall coefficient of Sb-doped tin oxide thin films.

| Samples | Resistivity (Ω.cm) | Conductivity $(\Omega.cm)^{-1}$ | Carrier concentration $(cm^{-3})$ | Hall mobility $(cm^2/Vs)$ |
|---|---|---|---|---|
| pristine $SnO_2$ | 3.22 x $10^3$ | 3.1 x $10^{-4}$ | 1.42 x $10^{12}$ | 1350 |
| 1%Sb: $SnO_2$ | 1.02 x $10^3$ | 1.01 x $10^{-3}$ | 3.31 x $10^{12}$ | 1806 |
| 3%Sb: $SnO_2$ | 0.22 | 4.51 | 1.53 x $10^{19}$ | 3.8 |
| 5%Sb: $SnO_2$ | 0.16 | 6.19 | 2.02 x $10^{19}$ | 2.0 |

### 3.4 Surface morphological and chemical elements analysis

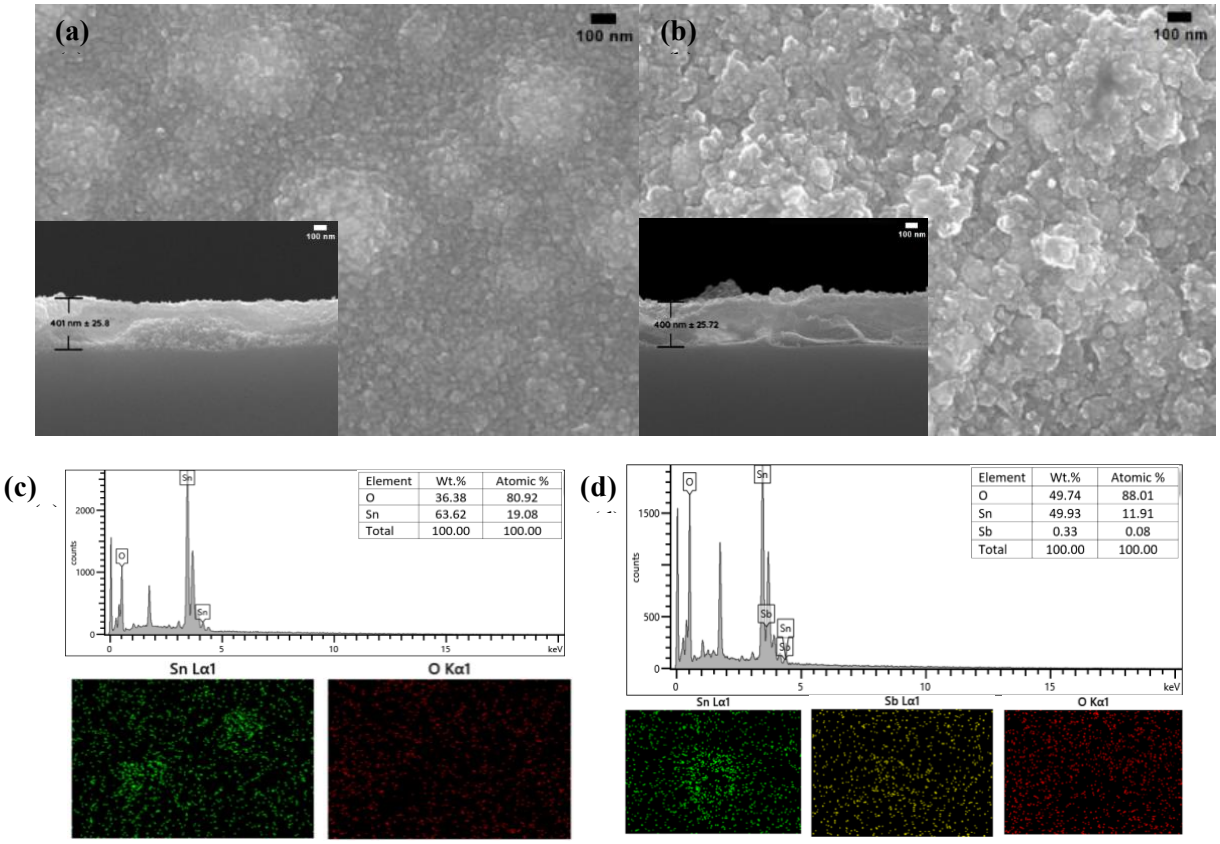


**Fig. 5.** FE-SEM micrograph of (a) pristine $SnO_2$ film (inset with cross-section micrograph), (b) 5% Sb doped $SnO_2$ film (inset with cross-section micrograph), and comparison of EDX results of (c) undoped and (d) 5% Sb doped $SnO_2$ films

In alignment with the electrical property results, the 5% Sb-doped $SnO_2$ thin film exhibited the highest electrical conductivity compared to the undoped film. To further examine the structural and compositional differences, surface morphology and elemental distribution of the pristine and 5% Sb-doped $SnO_2$ films were analyzed using Field Emission Scanning Electron Microscopy (FE-SEM) and Energy Dispersive X-ray Spectroscopy (EDX), as shown in Fig. 5. The FE-SEM micrographs revealed notable differences in surface texture between the two films. Cross-sectional measurements indicated that both the pristine and doped films had a comparable thickness of approximately 400 nm, suggesting that Sb doping does not significantly affect film thickness under the given synthesis conditions. The pristine $SnO_2$ film displayed relatively small and non-uniform grains across the surface, whereas the 5% Sb-doped $SnO_2$ film exhibited larger, irregularly shaped grains and increased surface roughness. The smoother surface and finer grains of the undoped $SnO_2$ may be responsible for its slightly higher carrier mobility, as fewer grain boundaries facilitate better charge transport, consistent with the crystallinity

results observed in XRD analysis [11]. In contrast, the rougher, more aggregated surface of the doped film is indicative of decreased crystallinity, also reflected in XRD results, and correlates with its lower mobility. This increased surface irregularity may stem from partial oxygen deficiency during annealing, which encourages higher Sb substitution into the lattice. Such substitution can disrupt the crystal structure and reduce crystallite size, ultimately affecting the film's mobility and increasing its electrical resistivity [9]. The EDX analysis confirmed the elemental composition of the films. For the pristine $SnO_2$ film, only tin (Sn) and oxygen (O) signals were detected, as expected. In contrast, the 5% Sb-doped $SnO_2$ film showed the presence of tin (Sn), oxygen (O), and antimony (Sb), confirming the successful incorporation of Sb into the film structure. The elemental mapping further demonstrated a relatively uniform distribution of Sb throughout the doped film, supporting the structural and electrical improvements observed.

### 3.5 Figure of Merit (FoM)

Based on the combined optical and electrical results, the overall performance of the films was evaluated in terms of the Figure of Merit (FoM), which describes the balance between visible light transparency and electrical conductivity [7]. The performance of transparent conductive oxide (TCO) thin films depends on key parameters, notably the optical transmittance at 550 nm and the sheet resistance. The FoM was calculated using Haacke's formula (Equation 5), and the results are presented in Fig. 6 and Table 4. The results show a significant improvement in FoM with increasing Sb dopant concentration. The pristine $SnO_2$ film exhibited the lowest FoM value of approximately $3.8 \times 10^{-10}$ $(\Omega \cdot cm^2)^{-1}$, indicating poor performance due to its high resistivity despite high transmittance. In contrast, the 5% Sb-doped $SnO_2$ film demonstrated the highest FoM of $5.98 \times 10^{-6}$ $(\Omega \cdot cm^2)^{-1}$, indicating a favorable combination of high electrical conductivity and adequate optical transmittance.

These findings confirm that Sb doping is a critical factor in enhancing the optoelectronic performance of $SnO_2$-based TCO films. The increased carrier concentration and improved conductivity with minimal compromise in visible light transparency contribute to a higher FoM, making Sb-doped $SnO_2$ a promising candidate for TCO applications in optoelectronic devices such as displays and solar cells.

$$\text{FoM } (\phi) = \frac{T^{10}}{R_s} \tag{5}$$

Where Φ is the fig. of merit, T is the transmittance at 550 nm, and $R_s$ is the sheet resistance.

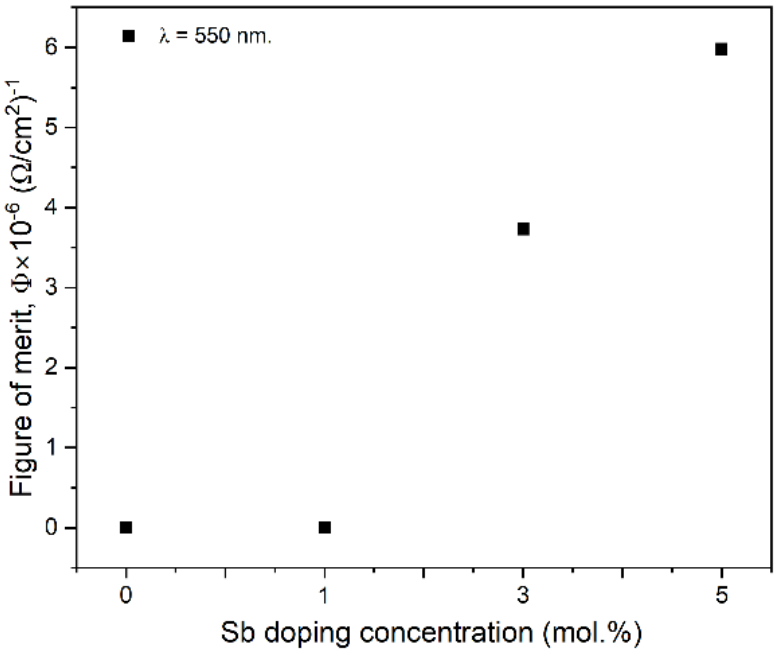


**Fig. 6.** Figure of Merit of transparent conducting oxide (TCOs), pure and Sb-doped $SnO_2$ thin films

**Table 4.** Comparison of electrical parameters: electrical resistivity, electrical conductivity, carrier mobility, carrier concentration, and Hall coefficient of Sb-doped tin oxide thin films.

| Samples | Transmission at 550 nm (%) | Sheet resistant $R_s$ ($\Omega.cm^2$) | Figure of merit (FOM, Φ) $(\Omega.cm^2)^{-1}$ |
|---|---|---|---|
| pure $SnO_2$: 10 layers | 72.6 | $1.07 \times 10^8$ | $3.8 \times 10^{-10}$ |
| 1% Sb doped $SnO_2$: 10 layers | 71.8 | $3.46 \times 10^7$ | $1.05 \times 10^{-9}$ |
| 3% Sb doped $SnO_2$: 10 layers | 69.8 | $7.37 \times 10^3$ | $3.73 \times 10^{-6}$ |
| 5% Sb doped $SnO_2$: 10 layers | 70.9 | $5.37 \times 10^3$ | $5.98 \times 10^{-6}$ |

## 4. Conclusion

In this study, Sb-doped $SnO_2$ thin films with varying Sb dopant concentrations and coating layers were successfully synthesized using the sol-gel method combined with spin-coating. All films exhibited a single-phase tetragonal rutile $SnO_2$ structure, as confirmed by XRD analysis. Increasing the Sb dopant concentration resulted in a decrease in crystallinity, attributed to lattice distortion caused by the incorporation of $Sb^{5+}$ ions, which also led to slight variations in the lattice parameters. Surface morphology analysis revealed uniform film coverage, with changes in grain size observed in FESEM micrographs. EDX elemental mapping confirmed the presence and uniform distribution of Sn, O, and Sb in the doped films. Optical analysis demonstrated a progressive increase in optical band gap values from 3.88 eV (undoped) to 4.05 eV (5% Sb), which can be explained by the Burstein–Moss effect due to increased carrier concentration. Electrical measurements showed that the lowest resistivity of 0.16 Ω·cm and the highest carrier concentration of approximately $2.02 \times 10^{19}$ $cm^{-3}$ were achieved at 5% Sb doping with 10 coating layers. However, the Hall mobility decreased to 2.0 $cm^2/V \cdot s$, indicating enhanced ionized impurity scattering. The optimal optoelectronic performance, expressed in terms of the Fig. of Merit (FoM), was found in the 5% Sb-doped $SnO_2$ film, reaching a maximum FoM of $5.98 \times 10^{-6}$ $(\Omega \cdot cm^2)^{-1}$. These findings demonstrate that Sb doping significantly improves the electrical conductivity while maintaining acceptable optical transparency, making Sb-doped $SnO_2$ a promising candidate for transparent conductive oxide (TCO) applications in optoelectronic devices such as displays, solar cells, and smart windows.

## Acknowledgments

This research has received support from the Nanotechnology and Materials Analytical Instrument Service Unit (NMIS) of the School of Integrated Innovative Technology (SIITec), King Mongkut's Institute of Technology Ladkrabang, for facility and analytical support.

## References

[1] Exarhos, G.J., & Zhou, X. (2007). Discovery-based design of transparent conducting oxide films. *Thin Solid Films, 515*(18), 7025-7052. DOI: 10.1016/j.tsf.2007.03.014.

[2] Hammad, T.M., & Hejazy, N.K. (2012). Retracted: Structural, electrical, and optical properties of ATO thin films fabricated by dip coating method. *International Nano Letters*, *2*, 7. DOI: 10.1186/2228-5326-2-7.

[3] Hossain, F., Shah, A. H., Islam, A., Rahman, S., & Hossain, S. (2020). Structural, morphological and opto-electrical properties of transparent conducting $SnO_2$ thin films: Influence of Sb doping. *Materials Research Innovations*, *25*(5), 300–309. DOI: 10.1080/14328917.2020.1801272.

[4] Nütz, T., & Haase, M. (2000). Wet-Chemical Synthesis of Doped Nanoparticles: Optical Properties of Oxygen-Deficient and Antimony-Doped Colloidal $SnO_2$. *The Journal of Physical Chemistry B*, *104*(35), 8430–8437. DOI: 10.1021/jp001932s.

[5] Luo, Y., Yang, J., Dai, X., Yang, Y., & Fu, S. (2009). Preparation and Optical Properties of Novel Transparent Al-Doped-ZnO/Epoxy Nanocomposites. *The Journal of Physical Chemistry C*, *113*(21), 9406-9411. DOI: 10.1021/jp901501z.

[6] Santibenchakul, S., Banchuen, S., & Chongsri, K. (2019). Influence of Sb dopant on Physical and Electrical Properties of Coprecipitated ZnO Nanoparticles. *Thai Journal of Nanoscience and Nanotechnology*, *4*(2), 1-5. https://ph05.tci-thaijo.org/index.php/TJNN/article/view/63.

[7] Fauzia, V., Yusnidar, M., Lalasari, L. H., Subhan, A., & Umar, A. A. (2017). High figure of merit transparent conducting Sb-doped $SnO_2$ thin films prepared via ultrasonic spray pyrolysis. *Journal of Alloys and Compounds*, *720*, 79-85. DOI: 10.1016/j.jallcom.2017.05.243.

[8] Lee, H.Y., Cai, Y., Bi, S., Liang, Y.N., Song, Y. & Hu, X. M. (2017). A Dual-Responsive Nanocomposite toward Climate-Adaptable Solar Modulation for Energy-Saving Smart Windows. *ACS Applied Materials & Interfaces*, *9* (7), 6054-6063. DOI: 10.1021/acsami.6b15065.

[9] Hossain, M. F., Shah, M. a. H., Islam, M. A., & Hossain, M. S. (2020). Transparent conducting $SnO_2$ thin films synthesized by nebulized spray pyrolysis technique: Impact of Sb doping on the different physical properties. *Materials Science in Semiconductor Processing*, *121*, 105346. DOI: 10.1016/j.mssp.2020.105346.

[10] Zheng, M., Ni, J., Liang, F., Wang, M., & Zhao, X. (2016). Effect of annealing temperature on the crystalline structure, growth behaviour and properties of $SnO_2$:Sb thin films prepared by radio frequency (RF)-magnetron sputtering. *Journal of Alloys and Compounds*, *663*, 371-378. DOI: 10.1016/j.jallcom.2015.12.037.

[11] Liu, L., Ueda, M., & Kawaharamura, T. (2023). Characterization and study of high conductivity antimony-doped tin oxide thin films grown by mist chemical vapor deposition. *RSC Advances, 20*(13), 13456-13462. DOI: 10.1039/D3RA00359K.

[12] Yang, Z., Zhang, M., Zhao, X., Guo, Z., Zeb, S., Jiang, W., Liu, T., Hu, R., & Jiang, X. (2023). Ammonia induced strong LSPR effect of chain-like ATO nanocrystals for hyperspectral selective energy-saving window applications. *Chemical Engineering Journal*, *479*, 147442. DOI: 10.1016/j.cej.2023.147442.

[13] Derrar, K., Zaabat, M., Rouabah, N., Nazir, R., Hanini, F., Hafdallah, A., Khan, S. A., Alsaiari, N. S., Katubi, K. M., & Abualnaja, K. M. (2022). Preparation of Sb:$SnO_2$ thin films and its effect on opto-electrical properties. *Journal of Materials Science Materials in Electronics*, *33*(13), 10142–10153. DOI: 10.1007/s10854-022-08004-3.

[14] Indrakanti, R., Brahmaji Rao, V. & Udaya Kiran, C. (2020) Optical parameters of gallium nitride doped ferrite–polypyrrole nanocomposites. *Journal of Materials Science: Materials in Electronics, 31*, 3238–3244. DOI: 10.1007/s10854-020-02872-3.